Original Article

A ternary model of proton therapy based on boron medium radiosensitization and enhancement paths: a Monte Carlo simulation

Xiaowa Wang[1,2,3,4], Liqun Shi[1,2], Xufei Wang[1,2], Lan Wang[3,4]

[1]Institute of Modern Physics, Fudan University, Shanghai, China; [2]Key Laboratory of Nuclear Physics and Ion-beam Application (MOE), Fudan University, Shanghai, China; [3]Shanghai Proton and Heavy Ion Center, Shanghai, China; [4]Shanghai Engineering Research Center of Proton and Heavy Ion Radiation Therapy, Shanghai, China

Contributions: (I) Conception and design: Xiaowa Wang, L Wang, Xufei Wang; (II) Administrative support: L Wang; (III) Provision of study materials or patients: Xiaowa Wang, L Shi, Xufei Wang; (IV) Collection and assembly of data: Xiaowa Wang, L Shi; (V) Data analysis and interpretation: Xiaowa Wang, Xufei Wang; (VI) Manuscript writing: All authors; (VII) Final approval of manuscript: All authors.

Correspondence to: Xiaowa Wang, PhD. Institute of Modern Physics, Fudan University, 220 Han-Dan Rd., Shanghai 200433, China; Key Laboratory of Nuclear Physics and Ion-beam Application (MOE), Fudan University, Shanghai 200433, China; Shanghai Proton and Heavy Ion Center, Shanghai 201315, China; Shanghai Engineering Research Center of Proton and Heavy Ion Radiation Therapy, Shanghai 201315, China. Email: wxwahmu@163.com; Lan Wang, MSc. Shanghai Proton and Heavy Ion Center, Kang-Xin Rd., Shanghai 201315, China; Shanghai Engineering Research Center of Proton and Heavy Ion Radiation Therapy, Shanghai 201315, China. Email: lan.wang@sphic.org.cn.

Background: To overcome proton therapy limitations [low linear energy transfer (LET) radiation with a relative biological effectiveness (RBE) typically ranging from 1.1 to 1.2], radiosensitization techniques can be employed to increase the radiosensitivity of tumor cells and improve the effectiveness of radiation therapy. In this study, we suggest using a boron-based medium to overcome the biological limitations of proton therapy. By inducing the hydrogen-boron fusion reaction ($p + {}^{11}B \rightarrow 3\alpha$) of incident protons and capturing thermal neutrons [${}^{10}B + n \rightarrow {}^{7}Li^{3+}$ (0.84 MeV) + ${}^{4}He^{2+}$ (1.47 MeV) + γ (0.477 MeV)], high LET α particles can be released. We propose a "ternary" radiotherapy model to enhance the biological effect of proton therapy.

Methods: Using Monte Carlo simulation, the possibility of interacting low-energy proton beams with ${}^{11}B$ and thermal neutrons with ${}^{10}B$ to produce α particles with higher RBE to enhance the biological effect of proton radiotherapy were investigated. And the number and location of α particles and thermal neutrons produced by the interaction of protons with natural boron had also been studied.

Results: Under the basic principle of the "ternary" radiotherapy model, comparative analyses of neutrons and α particles produced by proton beams of different energies incident on the phantoms, which were composed of boron isotopes of different concentrations in proportion to the phantoms, have shown that the α particle yield decreased with decreasing boron doping concentration, whereas the neutron yield increased with decreasing boron doping concentration. The distribution of thermal neutrons and α particles in the longitudinal direction of the proton beam were also studied, and it was found that the number of α particles produced was high at high boron concentrations, and the locations of α and thermal neutrons were close to the treatment target.

Conclusions: The proton therapy ternary model is theoretically feasible from the perspective of mathematical analysis and Monte Carlo simulation experiments.

Keywords: Boron; radiosensitization; ternary model; proton therapy; Monte Carlo simulation

Submitted Jun 28, 2023. Accepted for publication Sep 22, 2023. Published online Oct 17, 2023.
doi: 10.21037/tcr-23-1107
View this article at: https://dx.doi.org/10.21037/tcr-23-1107

Introduction

Background

The physical advantages of proton therapy in dose delivery are well-known. However, it is important to note that proton therapy is considered a low linear energy transfer (LET) (a physical quantity that characterizes the ability of beams to act on matter and is defined as the amount of energy transferred by a charged particle per unit length of path, i.e., L = dE/dL (L is the LET, dE is the energy delivered, dL is the unit length track of charged particles). The unit of LET is keV/m, which is an indicator of the quality of the beam) radiation with a relative biological effectiveness (RBE) typically ranging from 1.1 to 1.2. While proton therapy has shown clinical efficacy, its effectiveness in treating hypoxic or resistant tumors (such as lung adenocarcinoma, glioma, and soft tissue sarcoma) is limited compared to photon radiotherapy.

To overcome these limitations, radiosensitization techniques can be employed to increase the radiosensitivity of tumor cells and improve the effectiveness of radiation therapy. Radiosensitization techniques typically address two situations: (I) tumor hypoxia leading to radioresistance; and (II) the need to limit the dose to the surrounding normal tissues while still delivering a high enough therapeutic dose to the target area for improved clinical efficacy. These techniques can involve the use of drugs or physical pathways to enhance the radiation-killing effect on tumor cells.

Radiosensitizing agents (1), which include small molecules such as oxygen, nitroimidazole, curcumin, thymidine analogs, as well as large molecules like miRNA, oligonucleotides, proteins, and peptides, have limitations in their effectiveness due to poor specificity and the risk of off-target effects (2). While there have been significant advances in the use of metal nano-radiosensitizing and sensitizing therapeutic integration materials, particularly nanogold, their ability to enhance the effect of proton therapy is still limited (3). The reason for this limitation is that the secondary electron dose enhancement effect of nanogold radiosensitization under proton irradiation is not sufficient to directly damage the lethal target (DNA) in the nucleus of the irradiated cells. This is due to the low energy of the collisional ionization secondary electrons, which have a range of only 100 nm on the surface, and can only enhance the indirect contribution of the free radical effect by surface (collisional site) irradiation (3). As a result, the enhancement effect on the RBE of proton therapy is limited.

Rationale and knowledge gap

Sikora *et al.* and Yoon *et al.* proposed a novel approach to enhance proton therapy by releasing α particles from the p(^{11}B,α)2α reaction with the target region ^{11}B, based on the high LET α particle product (4 MeV) and the cross section (1.7 barn) of the p(^{11}B,α)2α reaction using 650 keV protons (4,5). Cirrone *et al.* reported the first enhancement of the p(^{11}B,α)2α reaction, showing that the presence of ^{11}B led to a significant increase in the biological effect of proton-irradiated cells, as demonstrated by the dose-survival curve and chromosomal aberration analysis of prostate cancer cells (DU145) and breast epithelial cells (MCF-10A) at different locations of the extended Bragg peak [spread out Bragg peak (SOBP)] (6). However, subsequent physical calculations and simulation studies led to the opposite conclusion, suggesting that although the p(^{11}B,α)2α reaction could produce α particles with high LET, the safe concentration of ^{11}B in the tumour target area may not be sufficient to induce a visible enhanced biological effect based on its reaction cross section and calculation results. It is worth noting that the p(^{11}B,α)2α reaction is conceptually similar to boron neutron capture therapy (BNCT) [^{10}B + n → α (1.47 MeV) + Li (0.84 MeV)], which

Highlight box

Key findings

- According to the principles of the proposed ternary radiotherapy modality approach, significant yields of and thermal neutrons were produced and their distribution were concentrated in the therapeutic target area.

What is known and what is new?

- To address the limitations of the biological effect of proton therapy, a boron-based medium was proposed to induce the release of high linear energy transfer (LET) α particles by the incident proton hydrogen-boron fusion reaction (p + ^{11}B → 3α) and thermal neutron capture [^{10}B + n → ^{7}Li^{3+} (0.84 MeV) + ^{4}He^{2+} (1.47MeV) + γ (0.477 MeV)].
- A "ternary" radiotherapy model was developed to enhance the biological effect of proton therapy.

What is the implication, and what should change now?

- The number and distribution of α particles and thermal neutrons produced by the "ternary" radiotherapy model approach were first investigated using Monte Carlo simulations. Proton therapy ternary model is theoretically feasible from mathematical analysis and Monte Carlo simulation experiments.

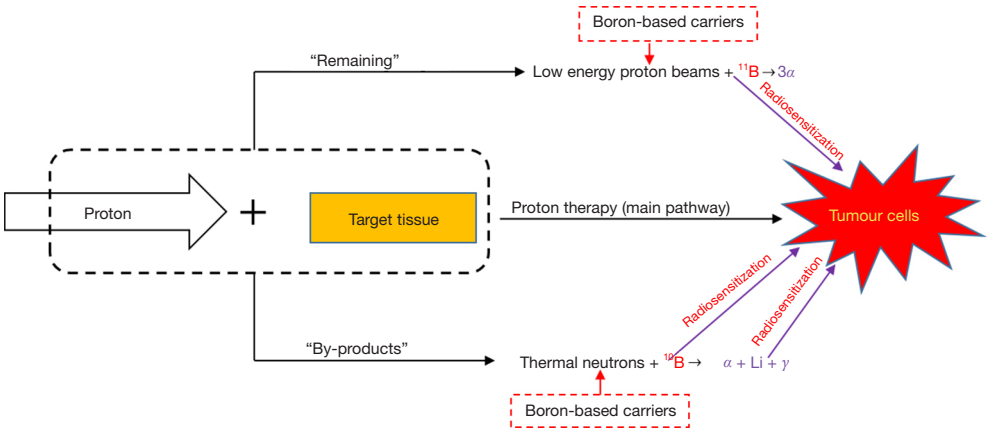

Figure 1 Schematic diagram of the sensitizing effect of boron-based proton "ternary" radiotherapy.

achieves higher biological effects by the reaction of thermal neutrons with ^{10}B (7). In contrast, the p(^{11}B,α)2α reaction is achieved by the nuclear fission reaction p + $^{11}B \rightarrow 3\alpha$(P-B), and energetic protons at the beam entry port can prevent the production of α particles in normal tissues.

Objective

In this paper, we proposed a "ternary" radiotherapy model, which was boron-based medium to induce the hydrogen-boron fusion reaction (p + $^{11}B \rightarrow 3\alpha$) of incident protons and thermal neutron capture [$^{10}B + n \rightarrow {}^{7}Li^{3+}$ (0.84 MeV) + $^{4}He^{2+}$ (1.47 MeV) + γ (0.477 MeV)]. And then the number and distribution of α particles and thermal neutrons produced by the interaction of radiotherapy protons with boron isotope-doped equivalent tissues of different ratios were first investigated by Monte Carlo simulation.

Proposed "ternary" model of proton therapy

During proton radiotherapy, not only does the interaction between the proton and the tumour target tissue destroy the tumour cells, but the biological effect of proton radiotherapy can also be enhanced in three ways. Firstly, the low-energy proton beam that remains after the initial interaction can produce particles with higher RBE through interaction with ^{11}B. Secondly, the nuclear reaction between the proton and the tumour target tissue can produce particles with higher RBE. Thirdly, the nuclear reaction between thermal neutrons and ^{10}B, one of the "by-products" of the proton-target interaction, can produce higher RBE particles and photons to enhance the biological effect of proton therapy. These three mechanisms together form a "ternary" model of proton radiotherapy. The three reaction pathways of the ternary model are shown in a schematic form in *Figure 1*.

Methods

In this study, the Monte Carlo simulation software tool FLUKA (8,9) and its interface FLAIR (10) (version 4.2) were used. The target material chosen for the simulation was mainly polymethyl methacrylate (PMMA) for the following reasons (11): firstly, it has a similar electron density and depth dose distribution to human tissue, although its elemental composition is not identical to that of human tissue. Secondly, it produces a similar range of fragmentation products to human tissue under the action of radiation. Finally, it is a commonly used target material in experimental procedures. PMMA has a density slightly less than that of water, 0.95 g/cm^3, the molecular formula is $C_5H_8O_2$, and the structural formula see *Figure 2*.

The FLUKA software tool was used to calculate the low-energy neutron cross section, with the ^{10}B, ^{11}B, and natural boron (^{N}B) LOW-MAT cards set at a temperature of 296 Kelvin (K). Boron was incorporated into PMMA materials at mass ratios ranging from 4,999:1 (200 ppm) to 1:1. The simulation was carried out in a homogeneous cube with dimensions of 250 mm × 250 mm × 250 mm and a bin setting of 1 mm in all three directions. The proton beam was scanned with a 5-mm pencil beam full width at half maximum (FWHM) and an energy range of 15–150 MeV. The recorded quantities during the simulations included the proton beam longitudinal dose distribution and Bragg

peak position, as well as the α and neutron counts along the proton beam longitudinal distribution.

The PMMA phantoms used in the experiment were not doped with boron substances but instead were composed of B-X (^{10}B, ^{11}B, and ^{N}B) with each having a mass percentage of PMMA:B-X =4,999:1, which corresponds to a percentage concentration of 200 ppm for each B-X in the PMMA.

The experiment was conducted with a 150 MeV proton beam incident on PMMA containing ^{10}B at varying concentrations.

Statistical analysis

To keep the error of the Monte Carlo simulation within 2%, the number of particles in the simulation was set to 5E+05. Preserve decimal places up to the fifth digit when processing resulting data.

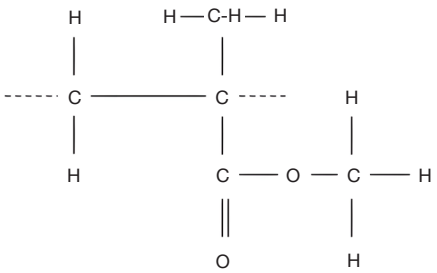

Figure 2 Structural formula of PMMA with the molecular formula ($C_5H_8O_2$). PMMA, polymethyl methacrylate.

Results

Analysis of α yield

The proton beam was incident from 15–150 MeV into each component of the phantom, and the amount of α particle production at the proton Bragg peak was recorded. The results showed that the highest α particle production was achieved at a proton energy of 60 MeV, as indicated by the dashed line in *Figure 3*. The trend of α particle production varied across B-X at different energies, but combining the α particle production at each energy, ^{10}B produced the most (2.40497E–06), followed by ^{11}B (2.38360E–06) and ^{N}B the least (2.36570E–06). Furthermore, at proton energies ≥30 MeV, the amount of α particle production by PMMA plus B-X was significantly greater than that produced by PMMA alone. The combined analysis suggests that the amount of α particle production is related to both the proton energy and B-X.

Description and analysis of results on 10B and its effects on α and neutron yields

The experiment was conducted and the resulting α and neutron production was recorded, as shown in *Table 1*. The analysis revealed that α production decreased with decreasing boron concentration for the same proton energy, while neutron production decreased with increasing boron

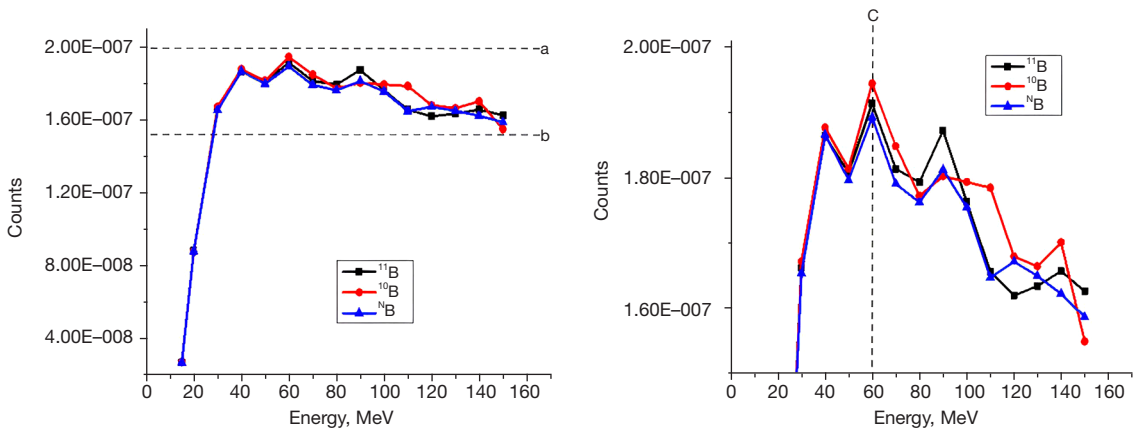

Figure 3 The amount of α produced by different proton incidence energies in the B-X and PPAM (200 ppm) phantoms. Dashed lines (a, b, and c) were used to highlight the role of the area and the location of the α peak. B-X is either ^{10}B, ^{11}B or ^{N}B. PMMA, polymethyl methacrylate; ^{N}B, natural boron.

Table 1 α and neutron peaks for different PMMA/^{10}B ratios

B:PMMA	Proton energy	Peak α counts	Peak neutron counts
^{10}B	150 MeV	2.47532E−07	3.61377E−08
6:1 (^{10}B)	150 MeV	2.38162E−07	3.63773E−08
5:1 (^{10}B)	150 MeV	2.16795E−07	3.74706E−08
4:1 (^{10}B)	150 MeV	2.13561E−07	3.78688E−08
3:1 (^{10}B)	150 MeV	2.09997E−07	3.85558E−08
2:1 (^{10}B)	150 MeV	2.02703E−07	4.08439E−08
1:1 (^{10}B)	150 MeV	1.89978E−07	4.85719E−08
1:2 (^{10}B)	150 MeV	1.70569E−07	4.47664E−08
1:8 (^{10}B)	150 MeV	1.70679E−07	7.02421E−08
1:10 (^{10}B)	150 MeV	1.65078E−07	8.87613E−08
1:11 (^{10}B)	150 MeV	1.61273E−07	1.35678E−07
1:4,999 (200 ppm) (^{10}B)	150 MeV	1.55267E−07	2.44118E−05

PMMA, polymethyl methacrylate.

concentration. This suggests that protons and boron work together to produce α particles with higher biological effects, and at higher boron concentrations, boron absorbs more neutrons and thus generates more α and fewer neutrons. The difference between the α peak position and the proton Bragg peak position varies for different boron isotopes and mass ratios of PMMA, but it is generally small and falls within the range of the proton Bragg peak position, as shown in *Figure 4*.

Analysis of α yield location

The amount of α produced and its corresponding position in the longitudinal direction of the proton beam incidence were recorded for the 150 MeV proton beam incident on the PMMA phantom and compared with the proton beam Bragg peak position. The positional differences between the α position and the Bragg peak position are shown in *Table 2*. While the differences between the two positions of the α peak position and the proton Bragg peak position for different mass ratios of ^{10}B to PMMA, they were small and essentially within the range of the proton Bragg peak position, as shown in *Figure 4*. Therefore, it can be inferred that the use of the "balance" α generated by the interaction of protons with boron drug carriers in proton radiotherapy can potentially further enhance tumor cell killing, leading to proton radiation sensitization.

Neutron position analysis

Table 3 presents the neutron yields and positions for a PMMA phantom with varying ^{10}B concentrations. While the peak neutron yield position was not located at the proton Bragg peak position, the neutron yield at the Bragg peak position remains at a certain level, albeit lower than the peak position. *Figures 5,6* illustrated the neutron number distributions and corresponding proton Bragg peak positions for two ^{10}B to PMMA concentration ratios, 1:11 and 1:4,999 (200 ppm), respectively. Despite the peak neutron production not being at the proton Bragg peak, a substantial number of neutrons were still present at the Bragg peak position, and they were all of the same order of magnitude.

Description and analysis of B-Xon α and neutron yields

Table 4 discusses the impact of B-X on α and neutron yields at the same proton energy. When the B-X to PMMA ratio is 1:11, the peak α production was lowest with ^{10}B, followed by ^{N}B, and highest with ^{11}B. However, when the B-X content was 200 ppm, the peak α production varied significantly among the three types. In terms of peak neutron production, the lowest amount was observed with ^{10}B, followed by ^{N}B, and the highest with ^{11}B when the B-X to PMMA ratio was 1:11. The difference between ^{11}B and the other two was more than two orders of magnitude.

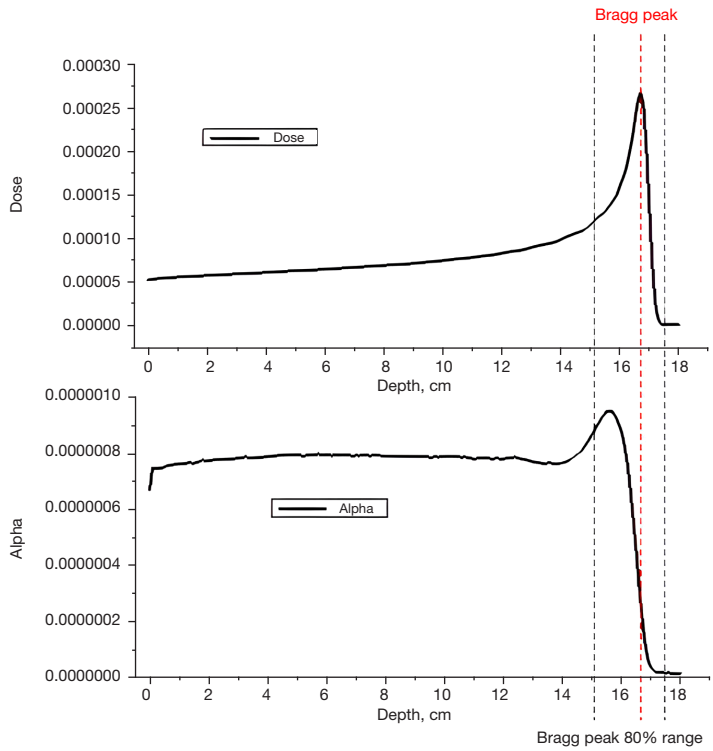

Figure 4 Analysis of the α position of the 150 MeV proton beam with boron production, the left side of the figure shows the position of the proton Bragg peak and the position of the produced α deposit.

Table 2 List of locations where different proportions of boron in PMMA produce peaks α

B:PMMA	Proton energy	Peak α location (cm)	Location of Bragg peak (cm)	Location gap (cm)
1:11 (^{N}B)	150 MeV	1.83	2.6	0.77
1:11 (^{11}B)	150 MeV	1.67	2.6	0.93
1:11 (^{10}B)	150 MeV	1.67	2.6	0.93
1:10 (^{10}B)	150 MeV	1.67	2.6	0.93
1:8 (^{10}B)	150 MeV	1.17	2.10	0.93
1:2 (^{10}B)	150 MeV	−1.33	−0.50	0.83
1:1 (^{10}B)	150 MeV	−4.83	−4.40	0.43
2:1 (^{10}B)	150 MeV	−4.17	−3.70	0.47
3:1 (^{10}B)	150 MeV	−4.17	−3.60	0.57
4:1 (^{10}B)	150 MeV	−4.33	−3.80	0.53
5:1 (^{10}B)	150 MeV	−4.50	−3.90	0.60
6:1 (^{10}B)	150 MeV	−4.00	−4.00	0.00
^{10}B	150 MeV	−4.50	−4.60	0.10

PMMA, polymethyl methacrylate; ^{N}B, natural boron.

Table 3 Neutron yield and location analysis

B:PMMA	Proton energy	Peak neutron	Location of peak neutron (cm)	Proton Bragg peak location (cm)	Neutron yield at the proton Bragg peak
1:11 (^{N}B)	150 MeV	6.72641E–07	–4.33	2.6	4.98710E–07
1:11 (^{11}B)	150 MeV	9.53065E–05	–4.17	2.6	7.06977E–05
1:11 (^{10}B)	150 MeV	1.35678E–07	–2.50	2.6	1.06851E–07
1:10 (^{10}B)	150 MeV	8.87613E–08	–2.67	2.6	7.01988E–08
1:8 (^{10}B)	150 MeV	7.02421E–08	–3.00	2.10	5.73477E–08
1:2 (^{10}B)	150 MeV	4.47664E–08	–3.83	–0.50	3.76428E–08
1:1 (^{10}B)	150 MeV	4.85719E–08	–6.33	–4.40	4.29006E–08
2:1 (^{10}B)	150 MeV	4.08439E–08	–5.67	–3.70	3.66115E–08
3:1 (^{10}B)	150 MeV	3.85558E–08	–5.67	–3.60	3.53427E–08
4:1 (^{10}B)	150 MeV	3.78688E–08	–5.67	–3.80	3.45245E–08
5:1 (^{10}B)	150 MeV	3.74706E–08	–5.67	–3.90	3.33587E–08
6:1 (^{10}B)	150 MeV	3.63773E–08	–5.50	–4.00	3.33831E–08
^{10}B	150 MeV	3.61377E–08	–6.00	–4.60	3.29080E–08

PMMA, polymethyl methacrylate; ^{N}B, natural boron.

When the B-X content is 200 ppm, the peak neutron amount was also highest with ^{11}B, followed by ^{N}B, and lowest with ^{10}B. However, the difference between the three was of the same order of magnitude. It should be noted that if the target phantom only contains pure ^{10}B, the difference in the number of neutrons produced compared to the PMMA content was also of the same order of magnitude.

Discussion

Key findings

Our findings showed that the α particle yield decreased with decreasing boron doping concentration, whereas the neutron yield increased with decreasing boron doping concentration. The α particles and thermal neutron products were predominantly distributed near the Bragg peak target area.

Strengths and limitations

The present study examines the neutron production of different isotopes and ratios of boron in equivalent tissue models, finding a significant neutron yield. For instance, at an incident proton beam energy =150 MeV and a ratio of ^{11}B:PMMA =1:11, the number of neutrons produced was 9.53065E–05, with the peak neutron production position around the proton Bragg peak. Notably, when using ^{10}B as a sensitizer, the number of neutrons produced was only 3.61377E–08 at the same proton energy and peak position, underscoring the importance of selecting the appropriate concentration of ^{10}B.

In this section, we discuss the potential benefits of using boron as a radiosensitizer to improve the effectiveness of proton therapy in killing tumor cells. One possible mechanism is the ability to concentrate protons at the subcellular level, particularly within the nuclei or DNA fragments of cancerous cells. To capitalize on this, our study proposes the use of a boron-based drug carrier to further enhance the radiosensitizing effect of proton radiotherapy in human tissue.

This paper focused on boron as a sensitizer to enhance the efficacy of proton radiotherapy. The principle of neutron capture therapy (NCT) was employed, which involved the reaction of ^{10}B with thermal neutrons [$^{10}B + n_{th} \rightarrow [^{11}B]^* \rightarrow \alpha + {}^{7}Li + \gamma$ (2.31 MeV)] (the asterisk means that the ^{11}B is "excited state") to generate charged particles with a higher relative biological effect (12,13). In contrast to traditional NCT, which utilized external thermal neutrons, our approach involved generating "extra" thermal neutrons during the proton therapy process. To achieve this, a non-toxic neutron trap containing ^{10}B was administered.

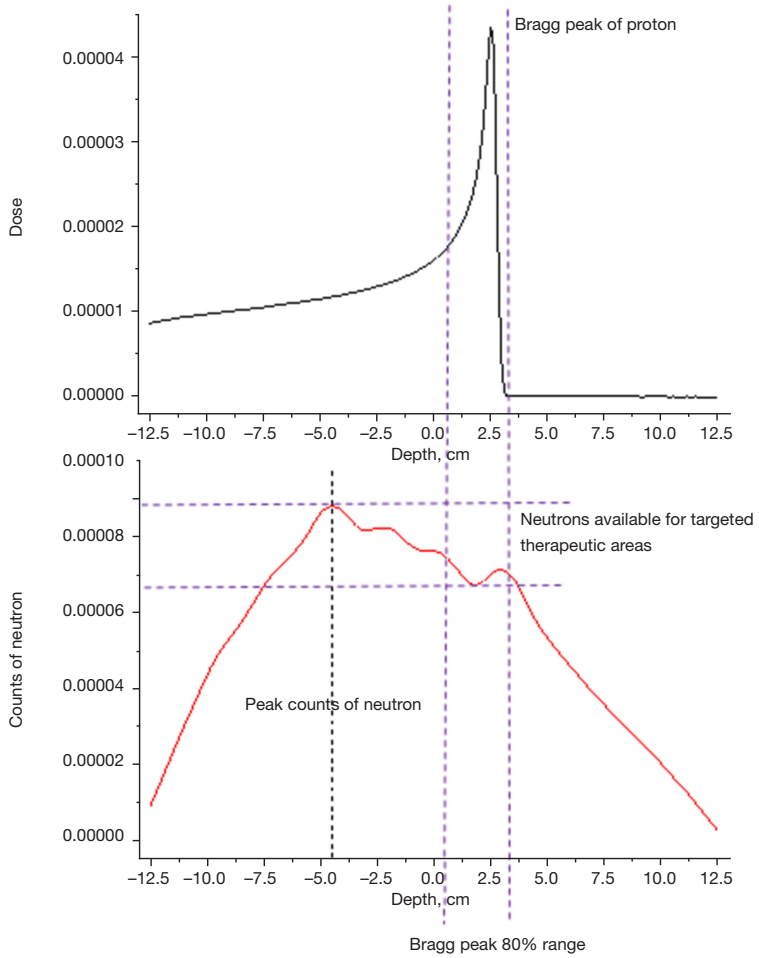

Figure 5 Neutron number yield and location distribution after irradiation of ^{10}B and PMMA moulds (mass ratio 1:11) with 150 MeV protons. PMMA, polymethyl methacrylate.

However, successful implementation of this approach depended on the production of sufficient thermal neutrons during proton therapy.

Explanations of findings

In this article, we performed a comparative analysis of neutron, α, and low-energy proton production for these models under varying proton beam energies and described the distribution of thermal neutrons and α particles in the longitudinal direction of proton beam incidence. The current limitations of the "ternary" mode of proton radiotherapy include the need for improved boron drug carriers to more accurately deliver the necessary boron concentration to the tumour target site, the large thermal neutron absorption cross section of α particles produced from higher concentrations of ^{10}B, and the requirement for further biological experimentation and clinical validation to support its effectiveness. Although drugs like sodium borocaptate (BSH) and boronophenylalanine (BPA) have been employed in clinical practice through BNCT, third-generation boron carriers are now being used, but additional research is necessary to optimize their efficacy. The "triadic" proton therapy model, structured into three pathways to enhance the radiation capacity of protons, exhibits limitations such as the absorption of a considerable number of thermal neutrons due to the significant thermal neutron absorption cross section of α particles produced from higher concentrations of ^{10}B. Therefore, the α particles generated by the interaction between the "remaining" proton and the boron drug carrier can be used to kill tumour cells further, thus enhancing the sensitivity of proton radiation therapy.

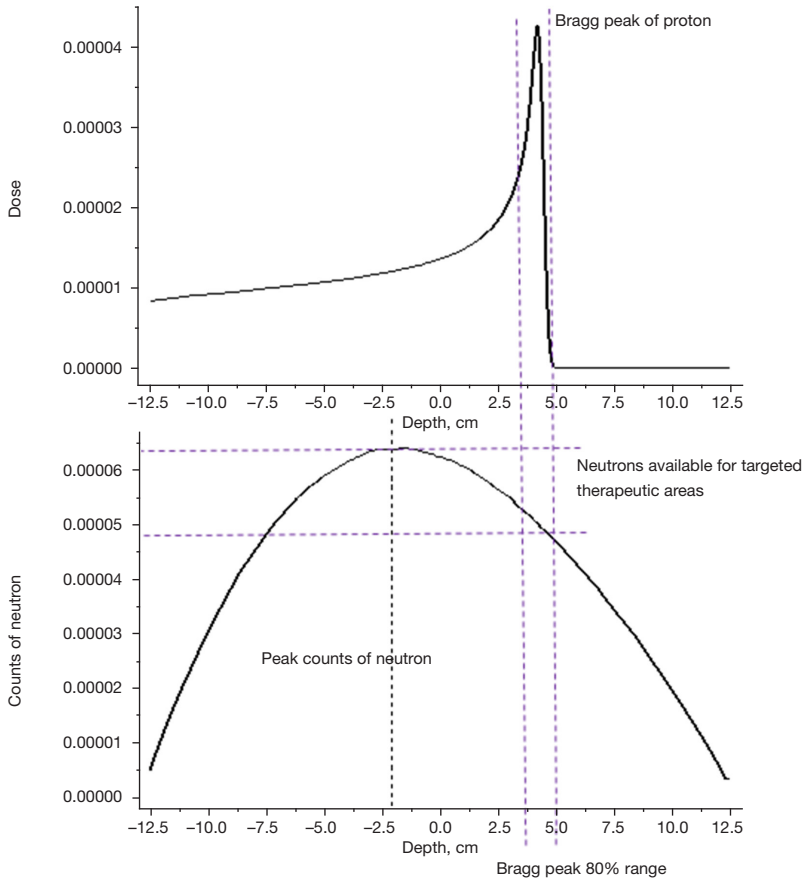

Figure 6 Neutron number yield and location distribution after irradiation of ^{10}B and PMMA moulds (200 ppm) with 150 MeV protons. PMMA, polymethyl methacrylate.

Table 4 PMMA with different B-X ratios producing peak alpha and neutrons

B:PMMA	Proton energy	Peak α counts	Peak neutron counts
1:11 (^{10}B)	150 MeV	1.61273E−07	1.35678E−07
1:11 (^{N}B)	150 MeV	1.65314E−07	6.72641E−07
1:11 (^{11}B)	150 MeV	1.70719E−07	9.53065E−05
1:4,999 (200 ppm) (^{10}B)	150 MeV	1.55267E−07	2.44118E−05
1:4,999 (200 ppm) (^{11}B)	150 MeV	1.54383E−07	6.42399E−05
1:4,999 (200 ppm) (^{N}B)	150 MeV	1.54479E−07	4.84083E−05
^{10}B	150 MeV	2.47532E−07	3.61377E−08

B-X is either ^{10}B, ^{11}B or ^{N}B. PMMA, polymethyl methacrylate; ^{N}B, natural boron.

Implications and actions needed

Although there is a current dispute regarding the theoretical and experimental outcomes, the notion of utilizing boron-based nuclear reactions to improve proton therapy has sparked numerous subsequent investigations (5,6,14-17). However, further exploration is necessary to resolve the controversy surrounding its physical feasibility and practical biological implications.

Conclusions

Proton therapy ternary model is theoretically feasible from mathematical analysis and Monte Carlo simulation experiments.

Acknowledgments

Funding: This work was supported by the National Natural Science Foundation of China (No. 12075063, 2021).

Footnote

Data Sharing Statement: Available at https://tcr.amegroups.com/article/view/10.21037/tcr-23-1107/dss

Peer Review File: Available at https://tcr.amegroups.com/article/view/10.21037/tcr-23-1107/prf

Conflicts of Interest: All authors have completed the ICMJE uniform disclosure form (available at https://tcr.amegroups.com/article/view/10.21037/tcr-23-1107/coif). The authors have no conflicts of interest to declare.

Ethical Statement: The authors are accountable for all aspects of the work in ensuring that questions related to the accuracy or integrity of any part of the work are appropriately investigated and resolved.

References

1. Wang H, Mu X, He H, et al. Cancer Radiosensitizers. Trends Pharmacol Sci 2018;39:24-48.
2. Tao YP, Zhao GP. Application of radiosensitizers in oncotherapy. Chinese Journal of Radiological Medicine and Protection 2019;39:715-20.
3. Feng AH, Li X, Wang XF, et al. Microdosimetric Evaluation on the Metallic Nanoparticle-Mediated Dose Enhancement in Radiotherapeutic Proton Irradiation. Chin Phys Lett 2018;35:068701.
4. Sikora MH, Weller HR. A New Evaluation of the 11B(p,α)αα Reaction Rates. J Fusion Energ 2016;35:538-43.
5. Yoon DK, Jung JY, Suh TS. Application of proton boron fusion reaction to radiation therapy: A Monte Carlo simulation study. Appl Phys Lett 2014;105: 223507.
6. Cirrone GAP, Manti L, Margarone D, et al. First experimental proof of Proton Boron Capture Therapy (PBCT) to enhance protontherapy effectiveness. Sci Rep 2018;8:1141.
7. Barth RF, Soloway AH, Fairchild RG. Boron neutron capture therapy of cancer. Cancer Res 1990;50:1061-70.
8. Ahdida C, Bozzato D, Calzolari D, et al. New capabilities of the FLUKA multi-purpose code. Front Phys 2022;9:788253.
9. Battistoni G, Boehlen T, Cerutti F, et al. Overview of the FLUKA code. Annals of Nuclear Energy 2015;82:10-8.
10. Vlachoudis V. FLAIR: a powerful but user friendly graphical interface for FLUKA. International Conference on Mathematics, Computational Methods & Reactor Physics (M&C 2009). Saratoga Springs, New York, May 3-7, 2009, on CD-ROM, American Nuclear Society, LaGrange Park, IL. 2009.
11. Matsufuji N, Fukumura A, Komori M, et al. Influence of fragment reaction of relativistic heavy charged particles on heavy-ion radiotherapy. Phys Med Biol 2003;48:1605-23.
12. Barth RF, Coderre JA, Vicente MG, et al. Boron neutron capture therapy of cancer: current status and future prospects. Clin Cancer Res 2005;11:3987-4002.
13. Barth RF, Vicente MG, Harling OK, et al. Current status of boron neutron capture therapy of high grade gliomas and recurrent head and neck cancer. Radiat Oncol 2012;7:146.
14. Giuffrida L, Margarone D, Cirrone GAP, et al. Prompt gamma ray diagnostics and enhanced hadron-therapy using neutron-free nuclear reactions. AIP Advances 2016;6:105204.
15. Xuan S, Zhao N, Zhou Z, et al. Synthesis and in Vitro Studies of a Series of Carborane-Containing Boron Dipyrromethenes (BODIPYs). J Med Chem 2016;59:2109-17.
16. Hideghéty K, Brunner S, Cheesman A, et al. (11)Boron

Delivery Agents for Boron Proton-capture Enhanced Proton Therapy. Anticancer Res 2019;39:2265-76.
17. Cammarata FP, Torrisi F, Vicario N, et al. Proton boron capture therapy (PBCT) induces cell death and mitophagy in a heterotopic glioblastoma model. Commun Biol 2023;6:388.

Cite this article as: Wang X, Shi L, Wang X, Wang L. A ternary model of proton therapy based on boron medium radiosensitization and enhancement paths: a Monte Carlo simulation. Transl Cancer Res 2023;12(10):2545-2555. doi: 10.21037/tcr-23-1107

